Aggregation Behavior of an Amphiphilic Graft Copolymer in Aqueous Medium Studied by Asymmetrical Flow Field-Flow Fractionation

Bengt Wittgren,[†] Karl-Gustav Wahlund,*[,†] Helene Dérand,[‡] and Bengt Wesslén[‡]

Department of Technical Analytical Chemistry, Chemical Center, University of Lund, P.O. Box 124, S-221 00 Lund, Sweden, and Department of Chemical Engineering II, Chemical Center, University of Lund, P.O. Box 124, S-221 00 Lund, Sweden

Received June 15, 1995; Revised Manuscript Received October 10, 1995[⊗]

ABSTRACT: Flow field-flow fractionation (FlFFF) was used to characterize the aggregation of a charged, amphiphilic copolymer, MMA 550, prepared from poly(styrene-*co*-methyl methacrylate-*co*-maleic anhydride) and poly(ethylene oxide) monomethyl ether. MMA 550 has a charged hydrophobic backbone and hydrophilic grafts which give the polymer a complex behavior in aqueous solution. FlFFF turned out to be a powerful tool for separation and size determination of different polymer aggregate populations in various media. The hydrodynamic diameter of the polymer was obtained from FlFFF measurements in water and pH-adjusted solutions. In pure water, the majority of the polymer molecules had a hydrodynamic diameter of 3−4 nm, which was also found at higher pH values (pH 9). When the pH was lowered, the hydrodynamic diameter increased rapidly. This suggested the formation of large micelles, probably polymolecular, as an effect of the reduced charge repulsion.

Introduction

Polymers that contain both hydrophobic and hydrophilic groups are amphiphilic and show a complex behavior in solution depending on their ability to associate and change conformation in media of different compositions. When the polymer contains charged groups, the situation may become even more complex. The complexity arises from the ability of the polymer to take part in both hydrophobic and hydrophilic type interactions, which can influence the molecular conformation as well as association with other polymer molecules.[1−7] Reports have been made on the occurrence of so-called "monomolecular" micelles as well as "polymolecular" micelles and also higher order aggregates, as illustrated in Figure 1.[1−3] Amphiphilic polymers will find use in many technical applications due to their ability to enrich at interfaces, thereby stabilizing interfacial structures.

In this work, the behavior in aqueous solution of an amphiphilic graft copolymer, (MMA 550) is examined. The polymer consists of a hydrophobic backbone containing styrene, methyl methacrylate, and maleic anhydride residues and hydrophilic grafts of poly(ethylene oxide) monomethyl ether (MPEO) (Figure 2). The grafting was done by opening of the succinic anhydride units with formation of an ester linkage to the MPEO graft and a carboxylic acid. Due to interactions between the hydrophobic parts of the backbone, an amphiphilic polymer tends to form a hydrophobic core with the hydrophilic grafts orientated toward the aqueous medium.[1,2,8] However, for the actual polymer, the backbone conformation will depend on the charge of the carboxylic acid groups. A charged backbone, obtained by dissociating the carboxylic groups through a pH increase, counteracts interactions between the hydrophobic styrene and methyl methacrylate units in the backbone. On the other hand high ionic strengths, obtained by salting-out agents, can decrease the charge repulsion of the backbone as well as the water solubilization of both the backbone and the hydrophilic grafts and may, accordingly, induce aggregation.[9−12] Consequently, the conformation of the polymer can depend on the pH and the ionic strength in the solution. Methods for measurement of changes in molecular or aggregate sizes are therefore important in order to understand the properties of an amphiphilic polymer.

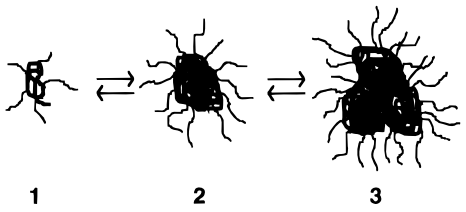

Figure 1. Illustration of the aggregation behavior of amphiphilic copolymers in aqueous solution. The hydrophobic parts (heavy line) form a dense core surrounded by the hydrophilic grafts (light line) in the micellous structures. Key: (1) monomolecular micelles; (2) polymolecular micelles; (3) clusters.

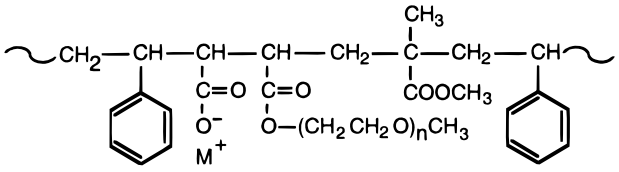

Figure 2. Schematic structure of MMA 550.

The complex interaction patterns put great demands upon a suitable characterization method. Methods such as dynamic light scattering (DLS), gel permeation chromatography (GPC), electron microscopy, and viscometry can be used to characterize properties such as hydrodynamic diameter, hydrodynamic volume, molecular weight, and colloidal particle size. However, every method suffers from various limitations. DLS is an excellent method to determine the average hydrodynamic diameters of monodisperse and relatively narrow sized monomodal distributions in a size range above about 5 nm.[13,14] With bi- or polymodal distributions DLS may meet difficulties in providing sufficient resolution and reliable size estimations depending on the level of ad-

[†] Department of Technical Analytical Chemistry.
[‡] Department of Chemical Engineering II.
[⊗] Abstract published in *Advance ACS Abstracts,* November 15, 1995.

0024-9297/96/2229-0268$12.00/0

vancement of the instrument. The lower size limit may be a problem in studies of smaller molecules and micelles. GPC is the standard method for determinations of molecular weight distributions but only for relatively low molecular weight polymers up to 10^6. It can hardly be used in the colloidal size range. Another problem may be adsorption to the stationary phase, which disturbs the size fractionation. Formation of aggregates large enough to be outside the resolution range of the GPC column is another limitation.[15] Such difficulties have appeared in previous attempts to characterize amphiphilic polymers.[1] Electron microscopy is very time-consuming in sample preparation and measurement of individual particle sizes. During sample preparation the polymer coils may collapse and the observed morphology will not necessarily be the same as in solution. Accordingly, this may lead to errors when micellar size and solution behavior are estimated.[5] Viscometry is a useful tool when examining the average molecular weight or major conformational variations but gives little information about size distributions and polymodality.[3,5]

Thus, it can be concluded that there is a need for a size characterization method which covers a wide size range, has good resolution, and is rapid. One method well suited for these demands is field-flow fractionation (FFF). It has, during a 25-year period of developement, reached a commercial status and has proven to be a powerful separation tool in applications to samples in the macromolecular, colloidal, and micron-size range.[16,17] The method is a chromatography-like separation procedure taking place in a thin channel through which the sample components are transported by a liquid carrier flow. While subject to such longitudinal transport the components are exposed to a transversal field which interacts with them so that they are driven to one of the walls which defines the channel. Because of the nature of the interaction with the field, the separation depends on a specific property of the components. This forms the basis of the methodology to function as a characterization method.

Several different types of fields have been described, such as sedimentation, thermal, electrical, and secondary flow, leading to the subtechniques sedimentation FFF, thermal FFF, electrical FFF, and crossflow FFF. The last mentioned technique, often simply called flow FFF (FlFFF), is used in the present study. It separates components according to differences in their diffusion coefficients which can be interpreted in terms of the hydrodynamic diameter, a size and shape dependent parameter. It is therefore a universal separation method in the sense that it fractionates any materials which have different diffusion coefficients. In practice, the method covers a size range from 1 nm up to approximately 50 μm. For example, FlFFF has shown the ability to separate, with excellent resolution, micron-sized polystyrene latex particles[18] as well as various proteins and aggregates of proteins with molecular weights down to 12 000.[19−21] Furthermore, most separations are fast, often requiring less than 10 min.

The majority of FlFFF studies have been made using aqueous carriers. Several types of water-soluble polymers such as poly(styrenesulfonate),[22−25] poly(2-vinylpyridine),[24,25] pullulans,[23] poly(ethylene oxide),[23] dextrans,[23] and poly(vinylpyrrolidone)[23] have been studied by FlFFF. There are basically no restrictions to changes in conditions such as pH, salt concentrations, and salt type. A few reports exist on using organic solvents as carriers for polymers such as poly(styrene) and poly(ethylene oxide).[26,27]

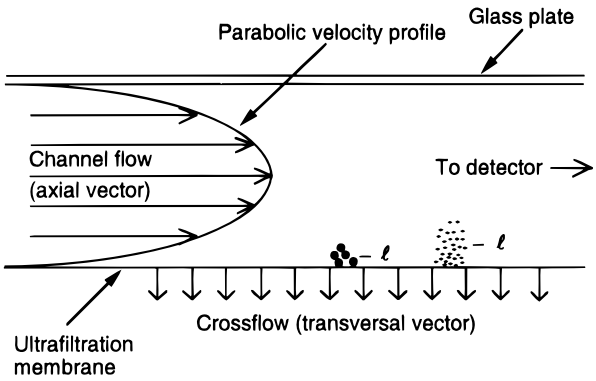

Figure 3. Principle of asymmetrical FlFFF illustrated for a short section of the total length of a channel. Sample components of various sizes are subjected to the crossflow (the transversal vector) and forced toward the ultrafiltration membrane. Diffusion will counteract this transport, and at equilibrium, the differently sized sample components will have different mean elevations *l* above the ultrafilter.

Thus, the generality and variability of the FlFFF method makes it well suited for size characterization of amphiphilic copolymers such as MMA 550. It not only covers the expected size range for monomolecular micelles, polymolecular micelles, and larger aggregates but also has the power to resolve these. Further, it allows easy changes of physico-chemical conditions such as ionic strength, pH, counterions, and sample concentration. In this way the method may serve to complement established techniques such as GPC and DLS and provide additional information when the results from these methods are difficult to interpret. Attempts to characterize micellization of amphiphilic polymers have been made by GPC, but the results are often questioned due to the disturbances by adsorption to the column particles.[1,2,28] In the present work we have examined the ability of FlFFF to give information on polymer behavior in aqueous solution by experiments both in pure water and in aqueous solutions of various pH values.

Theory of Asymmetrical FlFFF

Asymmetrical FlFFF is a further development of FlFFF with a solid upper wall (Figure 3).[29−31] The fractionations are performed by injecting samples into a thin rectangularly shaped channel through which an aqueous carrier flow is pumped. The bottom wall of the channel consists of an ultrafiltration membrane on top of a porous frit material through which a fraction of the carrier flow exits. This creates a secondary flow vector perpendicular to the primary longitudinal flow vector. The longitudinal flow, termed the channel flow, has a parabolic velocity distribution across the thickness dimension of the channel and carries the sample components down the channel to the outlet end where they are detected. The secondary flow, termed crossflow, drives any sample molecule or particle down to the membrane surface. This crossflow-induced drift will be counteracted by molecular diffusion caused by Brownian motion so that an exponential concentration distribution layer is established. The thickness of this layer therefore depends on the magnitude of the diffusion coefficients. A slowly diffusing component (high molecular weight) will accumulate relatively closer to the membrane surface than a more rapidly diffusing species because the slow diffusion is less effective in counteracting the crossflow-induced drift. The key to the fractionation is that the layers closer to the membrane

surface are subject to the lower longitudinal transport velocities in the parabolic velocity profile. The high molecular weight species therefore travel with lower speed through the channel, resulting in an elution order where components arrange themselves according to decreasing diffusion coefficients, *i.e.* increasing hydrodynamic size. This retention order is characteristic for sample materials in the submicron size range. A different retention order occurs in flow/hyperlayer FFF when the particle size exceeds about 1 μm.[32] In this case, the Brownian diffusion is negligible and the particle is so large that it is subjected to a hydrodynamic lift force which balances against the transverse crossflow force. The hydrodynamic lift forces increase with particle size, and therefore, the elution order will be the opposite, compared to the normal mode described above, with the largest component eluting first.

The basic theory of FlFFF has been described in detail several times, as applied to the "symmetrical" channel.[17,25,33] The theory of asymmetrical FlFFF differs somewhat from that of "symmetrical" channels and has been reported in detail previously.[29−31] The geometry of asymmetrical channels is sometimes different in that they are trapezoidal, which means that the breadth decreases on approaching the outlet end. This design was utilized in the present work. The theory for the trapezoidal channel has been developed before.[30,31]

Retention. The retention of a component in FFF is expressed by its retention ratio, R, which relates the retention time, t_r, to the void time, t^0.[29]

$$R = t^0/t_r \tag{1}$$

It is often useful to also express the retention as the reciprocal retention ratio, *i.e.* the ratio t_r/t^0, in which case the retention is quantified as a number of void times.

Another retention parameter is λ, which is defined by

$$\lambda = l/w \tag{2}$$

where w is the channel thickness and l is defined by

$$l = D/|u_o| \tag{3}$$

Here D is the diffusion coefficient of a component and $|u_o|$ is the velocity of the crossflow in close proximity to the surface of the accumulation wall. The parameter l is a measure of the distance from the accumulation wall of the component's exponential concentration distribution. This distance is a result of a balance between the drift toward the accumulation wall, caused by the crossflow velocity (the field), and the oppositely directed Brownian motion (*i.e.* diffusion). In an asymmetrical channel l approximately equals the center of gravity of the concentration distribution.

Parameter λ therefore depends on, in addition to the diffusion coefficient, the experimental variables which govern the crossflow velocity at the accumulation wall[29,33]

$$\lambda = DV^0/V_c w^2 \tag{4}$$

V^0 is the geometrical volume (void volume) of the channel, and V_c is the volumetric crossflow rate. It is obvious that the diffusion coefficient is the only property of the separated components which governs retention. Conversely, if the parameter λ can be determined from retention experiments, it is possible to determine the diffusion coefficient for a separated component.

The two retention parameters R and λ can be related using the expression[29]

$$R = \frac{6}{w}\frac{\int_0^w e^{(-x/l)B(x)}x\,dx - \frac{1}{w}\int_0^w e^{(-x/l)B(x)}x^2\,dx}{\int_0^w e^{(-x/l)B(x)}\,dx} \tag{5}$$

where

$$B(x) = 1 - \frac{x^2}{w^2} + \frac{x^3}{2w^3} \tag{6}$$

Equation 5 is applicable to the asymmetrical channel. Here x is the distance to the accumulation wall. The integrals have to be solved numerically due to the complexity of the exponent. Therefore this expression is used only when necessary, *i.e.* at weak retention. The numerical integration may be conveniently done by mathematics computer software (*e.g.* Mathematica or Matlab). For a range of values of w/l ($=1/\lambda$) the corresponding R values will be calculated. Among these, the one closest to the experimental R value is chosen in order to obtain the λ value needed.

At medium retention it is more convenient to use the following approximation of eq 5

$$R = 6\lambda\left[\coth\left(\frac{1}{2\lambda}\right) - 2\lambda\right] \tag{7}$$

A further approximation is useful at strong retention:

$$R = 6\lambda \tag{8}$$

Equation 5, 7, or 8 is used for estimations of λ from experimental R values. The λ value will be transformed to the diffusion coefficient, which in its turn provides the hydrodynamic diameter. The choice between eqs 5, 7, and 8 is therefore determined by the error which can be accepted in the finally estimated parameters.

Determination of the Hydrodynamic Diameter. First the thickness of the channel is determined using a procedure where the retention time of a compound of known diffusion coefficient is measured.[31] The void volume can now be obtained from the thickness multiplied by the area of the accumulation wall.

Next a determination of the void time is necessary. Because the channel is trapezoidal-shaped, one uses the expression[30]

$$t^0 = \frac{V^0}{V_c}\ln\left(1 + \frac{V_c}{V_{out}}\left[1 - \frac{w\left(b_0 z' - \frac{b_0 - b_L}{2L}z'^2 - y\right)}{V^0}\right]\right) \tag{9}$$

where, according to Figure 4, V_{out} is the channel outlet flow rate, z' is the distance from the inlet to the focusing point, L is the channel length, b_0 and b_L are the channel breadths at inlet and outlet, respectively, and y is the area cut off by the tapered inlet end. Now experimental R values are calculated from experimental retention times using eq 1.

The next step involves the estimation of λ from the R values using either eq 5, 7, or 8, depending on in which range of retention levels one is working. Table 1 gives the conditions in terms of retention ratio and t_r/t^0 which must be fulfilled in the estimation of λ at different levels of relative error. Once a λ value is obtained, the diffusion coefficient can be estimated using eq 4. To obtain hydrodynamic diameters, d_H, use is made of the

Table 1. Errors in the Estimation of λ and d_H Using the Two Approximations Eqs 7 and 8 for $R = f(\lambda)$

		level of relative error (%)					
		≤10		≤5		≤1	
param	eq	R	t_r/t^0	R	t_r/t^0	R	t_r/t^0
λ	7	≤0.41	≥2.4	≤0.29	≥3.4	≤0.14	≥7.2
	8	≤0.48	≥2.1	≤0.18	≥5.3	≤0.029	≥34
d_H	7	≤0.44	≥2.3	≤0.30	≥3.3	≤0.14	≥7.2
	8	≤0.44	≥2.3	≤0.17	≥5.7	≤0.029	≥34

Stokes−Einstein equation

$$D = kT/3\pi\eta d_H \tag{10}$$

where k is the Boltzmann constant, T is the absolute temperature, and η is the viscosity coefficient of the carrier liquid. If a particle is nonspherical, the hydrodynamic diameter thus obtained will be interpreted as an equivalent-sphere diameter. Combination of eqs 4 and 10 gives

$$d_H = \frac{kTV^0}{3\pi\eta V_c w^2}\frac{1}{\lambda} \tag{11}$$

which shows that the hydrodynamic diameter can be estimated for any λ value.

Obviously, the estimated hydrodynamic diameter is related to retention time. This becomes clear if eqs 1, 8, and 11 are combined to give

$$d_H = \frac{2kTV^0}{\pi\eta w^2 V_c t^0}t_r \tag{12}$$

The linear time scale of a fractogram can therefore be transformed to a linear scale of hydrodynamic diameters. However, it should be kept in mind that eq 12 was derived from the approximate retention ratio expression eq 8, which holds only for strong retention. On a linear size scale created from eq 12 applied to the strong retention range and then extrapolated into the weak retention range, the diameters in the weak retention range have an error which increases on approaching t^0, at which $d_H = 0$. Thus it is apparent that if the simple and useful approximation according to eq 12 is to be applied, one needs to avoid the weak retention range. Generally, this should be avoided anyway because of the low resolution in this range.[33,34] To enter the strong retention range, one should increase the crossflow rate as illustrated by the approximation

$$\frac{t_r}{t^0} = \frac{w^2}{6DV^0}V_c \tag{13}$$

which is obtained by combining eqs 10 and 12. V_c is normally increased by a higher inlet flow rate V_{in} at constant V_c/V_{out} ratio or by a decreased outlet flow rate V_{out} at constant V_{in}.[31] If size estimations in the weak retention range cannot be avoided, one is bound to estimate d_H by eq 11 using the better approximation (eq 7) or the complete expression (eq 5). If a maximal error in d_H of 5% can be accepted, the weak retention range can be defined as $t_r/t^0 < 5.7$.

For a truly concentration sensitive detector the response plotted *vs* the hydrodynamic diameter directly gives the mass distribution of the hydrodynamic diameter provided the molar absorptivity is constant.[34] However, in the nonlinear part of the size scale one must also correct mathematically the detector response curve, especially in close vicinity to t^0 ($t_r/t^0 < 2$), in order to obtain a correct size distribution curve.[34] If the detector response is partly turbidimetric, due to light scattering on larger colloidal particles, the mass distribution curve may become distorted. Another source of distortion may be the zone broadening occurring in the channel. This would contribute relatively little in the strong retention range. Channel zone broadening is well described in the weak retention range but difficult to model in the strong retention range due to broadening effects of unknown nature.[30,31]

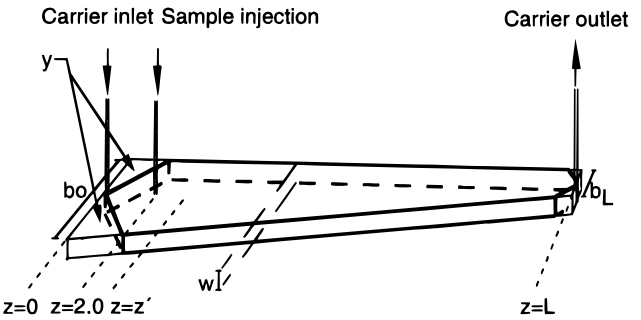

Figure 4. Channel geometry with thickness w and length L. The heavy lines illustrate the contours of the channel. b_0 and b_L are the breadths of a trapezoid at inlet and outlet, respectively, and y is the area cut off by the tapered inlet end. z' is the position of the sample zone during the relaxation/focusing. The sample injection inlet is placed 2.0 cm from the carrier liquid inlet.

The results of the FlFFF separations are presented below as fractograms where the uncorrected detector response (photometric absorbance) at the channel outlet is plotted *vs* retention time and/or hydrodynamic diameter. The various size populations observed are characterized by the hydrodynamic diameter estimated at the peak maxima.

Experimental Section

Materials. The preparation of the anionic graft copolymer MMA 550 was recently published.[35] The backbone polymer was prepared through solution terpolymerization of styrene, methyl methacrylate, and maleic acid. The terpolymer obtained consisted of 50 mol % styrene, 18 mol % methyl methacrylate, and 32 mol % maleic anhydride, as determined by NMR. Poly(ethylene oxide) monomethyl ether (MPEO) of molecular weight 550 was grafted onto the backbone polymer in solution through reaction with the anhydride groups. In this reaction one ester group was formed together with a carboxylic acid group. The graft copolymer was purified through dialysis in aqueous solution. The graft copolymer contained 28% w/w of MPEG and had a molecular weight of 135 000 calculated from GPC measurements of the backbone and NMR spectra of the graft copolymer. The polymer was obtained in its acidic form in water (7 mg/mL), and the pH was about 6.5. Before injection, the polymer was diluted in the actual carrier or in water.

Field-Flow Fractionation Method. The asymmetrical separation channel assembly was previously reported by Litzén.[36] All experiments were carried out using the same design. The accumulation wall consisted of an ultrafiltration membrane made of regenerated cellulose (NADIR UF-C-10), with a molecular weight cutoff of 10 000 (Hoechst AG, Wiesbaden, Germany). A spacer, made of PTFE (poly(tetrafluoroethylene)), was placed on the top of the membrane and had a cut forming the trapezoidal channel geometry, as seen in Figure 4. The channel length L was 28.5 cm. The trapezoid breadths b_0 and b_L were 2.1 and 0.47 cm, respectively. The area y cut off at the tapered inlet end was 2.1 cm^2, and the total area of the membrane enclosed by the spacer was 34.6 cm^2. The channel thickness w was calibrated with ferritin (Pharmacia, Uppsala, Sweden) to 0.0105 cm,[31] which gives a channel volume V^0 of 0.363 mL. The focusing point z' was determined with ferritin to 2.3 cm.[21] The membrane was

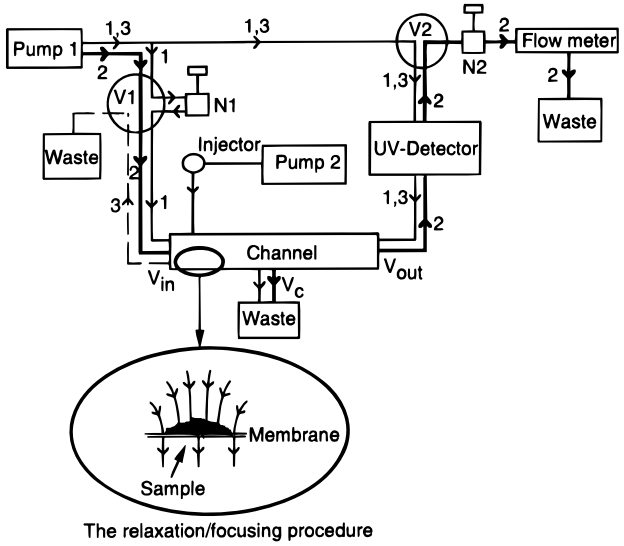

Figure 5. Schematic drawing of the instrumental setup. Pump 1 delivers the carrier liquid, and pump 2, the sample injection liquid. The motor-driven valves V1 and V2 determine the flow directions in the system. Initially, flow from pump 2 transports the sample to the channel during the injection/relaxation/focusing (1, light arrows). The carrier flow will enter the channel from both the inlet and outlet end and will exit only through the membrane. The flow rate from each direction is determined by the needle valve N1 so that the two flow streams meet near the injection position. This drives the sample axially to a focusing point[20,29] and transversally to the membrane surface where it becomes relaxed to a steady-state transversal concentration distribution profile under the influence of the transversally directed crossflow vector. The elution phase starts by changing flow directions (2, heavy arrows). Carrier with the flow rate V_{in} enters the channel and is divided into axial flow and crossflow (flow rate V_c). The outlet flow rate (V_{out}) is now measured by the flow meter and can be adjusted with the needle valve, N2. The fractionation is finished with a rinsing phase using backward flow of carrier liquid through the channel (3).

supported by a plane ceramic frit placed in a Lucite (poly(methyl methacrylate)) block, and the whole set was clamped together with bolts tightened by approximately 2.2 Nm.

The instrumental setup is schematically drawn in Figure 5 and has been described in detail previously.[21,31,36] The two pumps (pump 1 for carrier flow and pump 2 for injection flow) were both Kontron HPLC-pump 420 (pumphead M, 0.01−10 mL/min) (Kontron Instruments, Zurich, Switzerland). The sample injector was a Rheodyne 9125 syringe injector (Rheodyne Inc., Cotati, CA) with a 20 μL sample loop. Two motor-driven valves, denoted V1 and V2 in Figure 5, directed the flows delivered by pump 1. V1 was a Valco E-CST 4UV multiposition valve, and V2 was a Valco E C4W 2 position valve (Vici AG, Valco Europe, Schenkon, Switzerland). The photometric detector was a Pharmacia Monitor UV-M (Pharmacia LKB Biotechnology, Uppsala, Sweden) using a wavelength of 254 nm. The outlet flow rate was continuously monitored by a PhaseSep liquid flow meter (Phase Separations Ltd., Queensferry, U.K.). Two fine metering needle valves (Hoke Valve 1656 G2YA, Hoke Inc., Cresskill, NJ) were used: one regulated the flow directions at injection/relaxation/focusing, and the other regulated the outlet flow. The flow rates delivered by pump 1 and the motor valves V1 and V2 were directed by a Kontron Data System 450-MT2 (Kontron Instruments, Zurich, Switzerland), which also collected signals from detector and flow meter, respectively.

A complete fractionation consisted of three experimental phases, namely injection/relaxation/focusing, elution, and backward rinsing.[31] Each fractionation was initiated by a sample injection and the relaxation/focusing of the injected sample. During this first phase, the pump flow was directed by V1 and V2 according to Figure 5. This procedure was carried out for 1 min totally at a flow rate of 2 mL/min, and the sample injection was made during the first 30 s with a

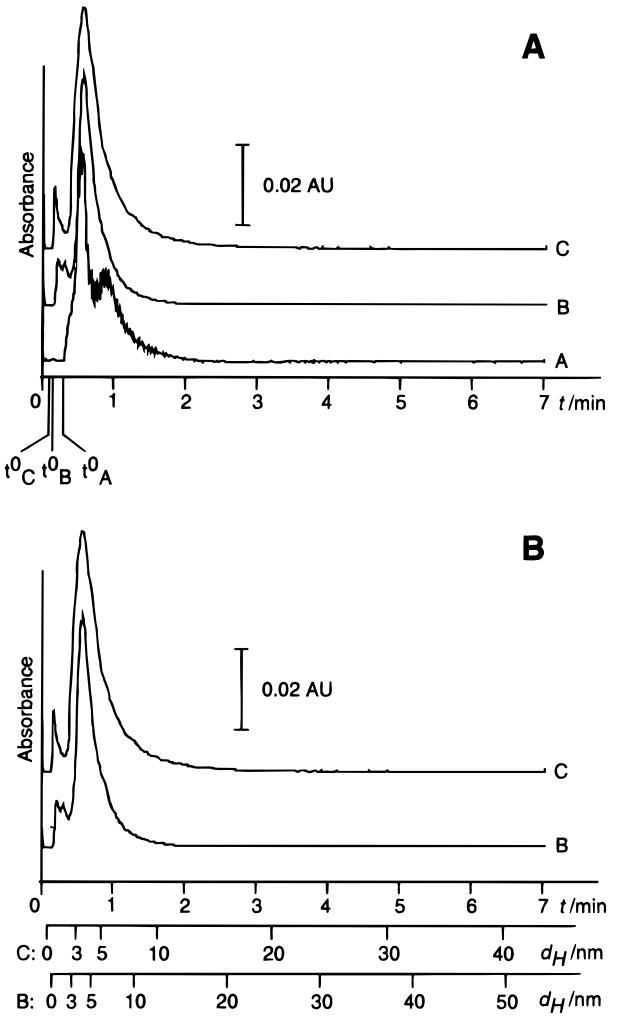

Figure 6. (A) Fractograms of MMA 550 obtained in pure water. The t_r/t^0 ratio is increased as the inlet flow rate increases. Conditions: (A) V_{in} = 3.0 mL/min, V_{out} = 0.3 mL/min, V_c/V_{out} = 9, t^0 = 0.30 min, t_r/t^0 = 1.9; (B) V_{in} = 6.0 mL/min, V_{out} = 0.5 mL/min, V_c/V_{out} = 11, t^0 = 0.15 min, t_r/t^0 = 3.8; (C) V_{in} = 10.0 mL/min, V_{out} = 0.5 mL/min, V_c/V_{out} = 19, t^0 = 0.10 min, t_r/t^0 = 5.5. Sample: MMA 550 diluted in water to 1.8 mg/mL. The relaxation/focusing time was 1 min. (B) Retention times of fractograms B and C converted into hydrodynamic diameters.

flow rate of 0.2 mL/min. Directly after the injection/relaxation/focusing phase the valves were switched for elution phase positions (Figure 5) and the flow rate from pump 1 was simultaneously changed to the actual V_{in}. After each fractionation, the carrier liquid was directed backward through the channel for 2 min at 6 mL/min in order to remove sample material left in the channel. This flushing was usually done with the actual carrier liquid, but at obvious pollution of the membrane surface, ethanol/water (70/30, v/v) was used. The retention times (t_r) were measured from the peak apices in the obtained fractograms. The void time t^0 for each fractionation was calculated using eq 9.

The carrier liquids were pure water, water modified with NaOH to pH 8.7, water modified with HCl to pH 5.7, 4.6, 4.0, 3.7, and 3.4, and 1 mM sodium phosphate buffers at pH 9.0, 5.0, and 3.0. The phosphate buffers, prepared from mono- or disodium phosphates, were adjusted to the actual pH using either phosphoric acid or sodium hydroxide. The temperature in the carrier liquid varied between 23 and 24 °C.

Results and Discussion

Water as Carrier Liquid. Figure 6 demonstrates a sequence of experiments suitable to perform when an unknown sample is analyzed. Initial conditions should be chosen so that rather low retention times are

obtained on the basis of some estimation of the molecular size of the polymer. In this way one is sure to observe even associates of the polymer which, due to their larger size, always have higher retention times than the single polymer molecule. If the size of the polymer has been overestimated, the retention time will be very low and close to the void time. Fractogram A in Figure 6A illustrates this case where the sample response was not even resolved from the "void peak", which often appears at the void time, t^0. An improved resolution from the void peak can be obtained by increasing V_{in} (and consequently V_c), as in fractogram B, whereby the void time decreases but the sample retention time is kept almost constant. A further improvement is observed in fractogram C, which shows that the polymer is represented by one single dominating size population.

The retention times for fractograms B and C were transformed into hydrodynamic diameters, as shown in Figure 6B. The size scale was drawn linearly for $t_r/t^0 \geq 5.7$. In the weak retention range the scale becomes nonlinear and the scale marks shown are obtained on the basis of eq 5, *i.e.* without error. In the following figures, all size scales were treated similarly so that the maximal error is 5%.

According to Figure 6B, the peak maximum of C corresponds to 3 nm and of B to 4 nm. The observed difference is thought to be due to experimental errors. It seems probable that this peak represents a population of single polymer molecules, which most probably are present in some micellar conformation.[1−3,5,6,8,9,28,37,38] An expanded conformation would probably lead to much larger size estimations relative to the molecular weight and the charge of the polymer. No other peaks were detected in the fractograms shown in Figure 6. This indicates that any polymer aggregates present either would represent a very small, nondetected fraction of the sample or are of such large size that they become forced too close to the accumulation wall, resulting in excessive retention times, retention levels, and zone broadening in the channel.[21] In the latter case the proper action would be to decrease the retention time for all components by a decrease of the V_c/V_{out} ratio at a constant V_{in}.[29] This leads to a decrease of the retention levels (t_r/t^0) as well (*cf.* eq 13). Such experiments did not show any new populations.

If the expected retention times are reasonable but the retention levels are too high, the latter can be decreased through a decrease of the crossflow rate V_c. If this is obtained by a decrease of the inlet flow rate V_{in} while keeping the ratio V_c/V_{out} constant, the retention time will be unchanged. In the fractogram this results in a shift of the void time to higher values while well-retained components keep their retention times. Such experiments with increased detection sensitivity and lower inlet flow rate gave a second small peak corresponding to approximately 20 nm (Figure 7) in size. The population in this size range may be polymolecular associates of the single polymer molecule. Compared to the main peak this second peak represented only a small fraction of the polymer, a fact that demands proper experimental conditions if this peak would be resolved from the main peak and from the noise. A conclusion is that experiments using different flow conditions are needed to give information regarding these two polymer populations.

pH-Adjusted Carrier Liquids. The polymer backbone contains carboxylic acid groups. Thus, the net charge of the molecules will depend on the pH in the solution. Consequently, the formation of aggregates,

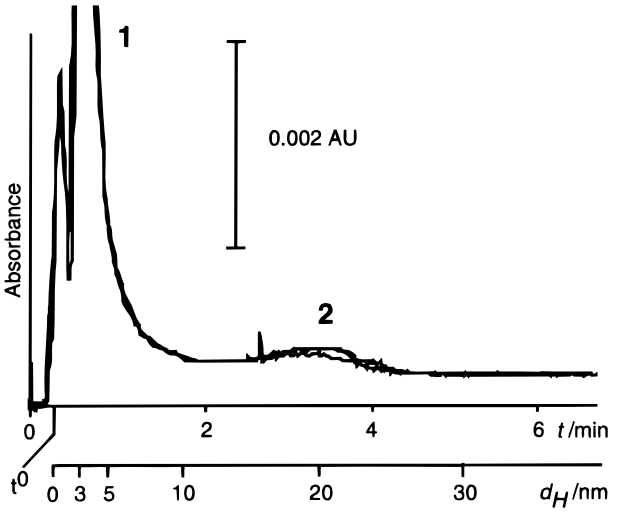

Figure 7. Detection of assumed polymolecular micelles in pure water as carrier. Peaks 1 and 2 may represent monomolecular micelles and polymolecular micelles, respectively. V_{in} = 4.0 mL/min, V_{out} = 0.2 mL/min, V_c/V_{out} = 19, and t^0 = 0.27 min. Sample: MMA 550 diluted in water to 1.8 mg/mL. The relaxation/focusing time was 1 min. The overlay of two parallel runs illustrates the good reproducibility which was also characteristic of all other fractgrams.

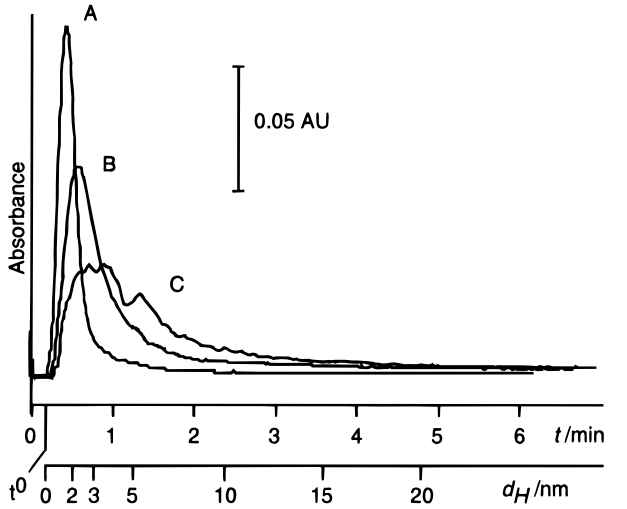

Figure 8. Fractograms of MMA 550 obtained in a carrier liquid containing 2.00 μM HCl, pH 5.7, using different relaxation/focusing times: (A) 1 min, (B) 3 min; (C) 8 min. There is a shift to larger sizes when the relaxation/focusing time is increased. V_{in} = 8.0 mL/min, V_{out} = 0.1 mL/min, V_c/V_{out} = 75, and t^0 = 0.18 min. Sample: MMA 550 diluted in the carrier to 0.7 mg/mL.

which mainly depends on the ability of the backbone chains to interact, would also be pH dependent. In the aforementioned experiments using unbuffered medium the polymer was probably partly ionized. In order to study the effect of a change in the net charge, the pH of the carrier was adjusted. Different amounts of hydrochloric acid and sodium hydroxide were therefore added to the carrier. The reason for choosing strong acids and bases for the pH adjustments was to avoid higher concentrations of buffer salts, which would have increased the ionic strength and therefore caused shielding effects. The solubility of the poly(ethylene oxide) chains may also decrease in high concentrations of "salting-out" salts. Six pH values from 8.7 down to 3.4 were tested, and the results from pH 5.7 and 4.6 are illustrated in Figures 8 and 9. One further experimental parameter was also tested, namely the sample

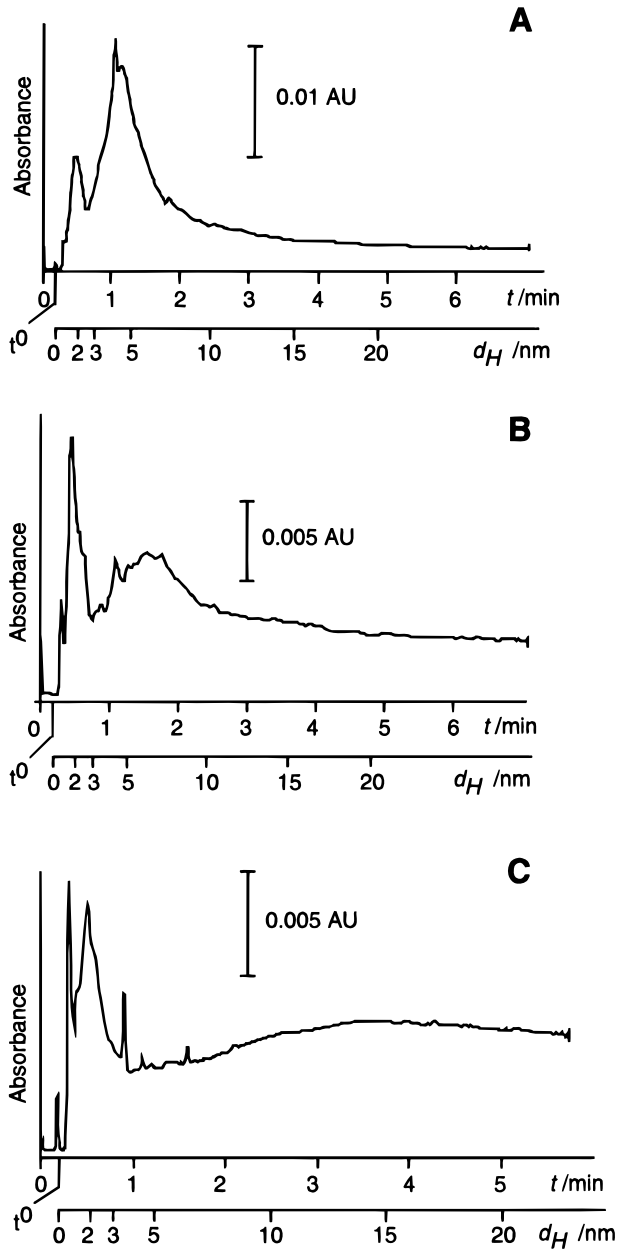

Figure 9. Fractograms of MMA 550 obtained in a carrier liquid containing 23.0 μM HCl, pH 4.6, using different relaxation/focusing times: (A) 1 min; (B) 3 min; (C) 8 min. Longer relaxation/focusing times result in a growth in size. $V_{in} = 8.0$ mL/min, $V_{out} = 0.1$ mL/min, $V_c/V_{out} = 73$, and $t^0 = 0.19$ min. Sample: MMA 550 diluted in the carrier to 0.7 mg/mL.

dilution medium. The original polymer samples were diluted alternatively by water or by the pH adjusted carriers before injection. The diluted samples were then injected in the actual pH-adjusted carrier. This was done in order to study the influence of the sample dilution medium on the FlFFF results. No such influence was observed. Obviously, the equilibration of thesample with the carrier medium during the 1-min relaxation/focusing procedure was sufficient. During the relaxation/focusing procedure the sample becomes flushed with the new medium while it is immobilized above the membrane surface. Different relaxation/focusing times were also examined to reveal if the time spent during these special conditions would influence the polymer aggregation.

Characteristically, the fractograms at higher pH values showed the presence of the supposedly monomolecular polymer population at hydrodynamic diameters around 2−3 nm. At pH 8.7 and 5.7 the fractograms

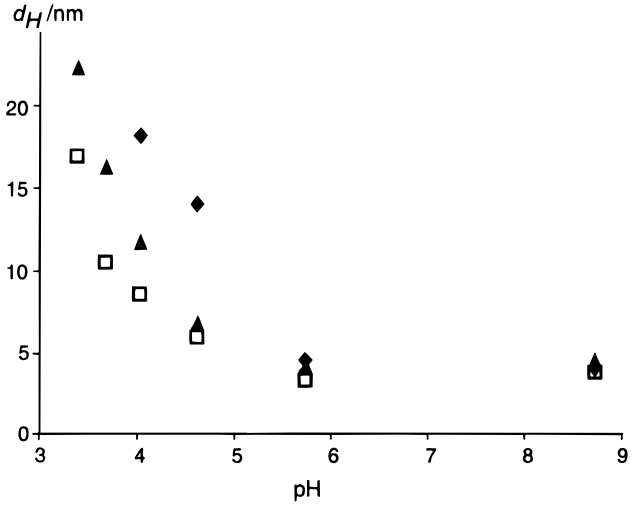

Figure 10. Influence of the relaxation/focusing time on the hydrodynamic diameter at different pH's. Relaxation/focusing time: 1 min (□), 3 min (▲), and 8 min (◆). Carriers were dilute NaOH (pH 8.7) and dilute HCl (pH 5.7, 4.6, 4.0, 3.7, and 3.4). Sample: MMA 550 diluted in the carrier to 1.8 mg/mL.

were very similar to those in pure water. The relaxation/focusing time influenced the peak shape only at pH 5.7, where a slight shift to larger sizes was noted (Figure 8). At a carrier pH of 4.6 the appearance of the fractogram was significantly different (Figure 9). At a relaxation/focusing time of 1 min (Figure 9A) two peaks occurred, one close to 2 nm and another slightly above 4 nm. The peak representing the smaller size can be assumed to be due to monomolecular micelles, and the larger one may represent a new population, most probably a polymolecular one. However, at longer relaxation times (3 and 8 min) the retention times for the large-sized population increased to values corresponding to hydrodynamic diameters up to around 15 nm. In Figure 10 the hydrodynamic diameters obtained (as estimated for the large-sized peak) are plotted for 1, 3, and 8 min relaxation/focusing times at the different pH values employed. It is evident that the decrease in pH causes a growth in aggregate size which seems to be further amplified by an increase in the relaxation/focusing time.

Our interpretation of these observations is that the polymer shows an increased association in a more acidic medium. It seems reasonable that this behavior is caused by the backbone being less charged at low pH values, and therefore hydrophobic backbone interactions become facilitated with polymolecular associations as a result. This explanation is also supported by the fact that at pH 8.7, where the polymer backbone carries more charge, the aggregate size was unchanged even at longer relaxation/focusing times. It is even possible that the internal structure of the monomolecular micelles changes, which may explain the slight decrease in the hydrodynamic diameter for the first population at lower pH. At pH 8.7, however, the monomolecular micelles seem to be of the same size as in pure water, 3 nm.

Furthermore, the increased sizes of the proposed polymolecular populations, observed on increasing the relaxation/focusing time, were only observed in acidic medium. An interpretation of this effect needs some understanding of the experimental procedure. During the relaxation/focusing, three different experimental parameters change. First, if the sample medium is not the same as the carrier, the time for equilibration of the polymer with the new medium increases when the relaxation/focusing time is increased. This can lead to

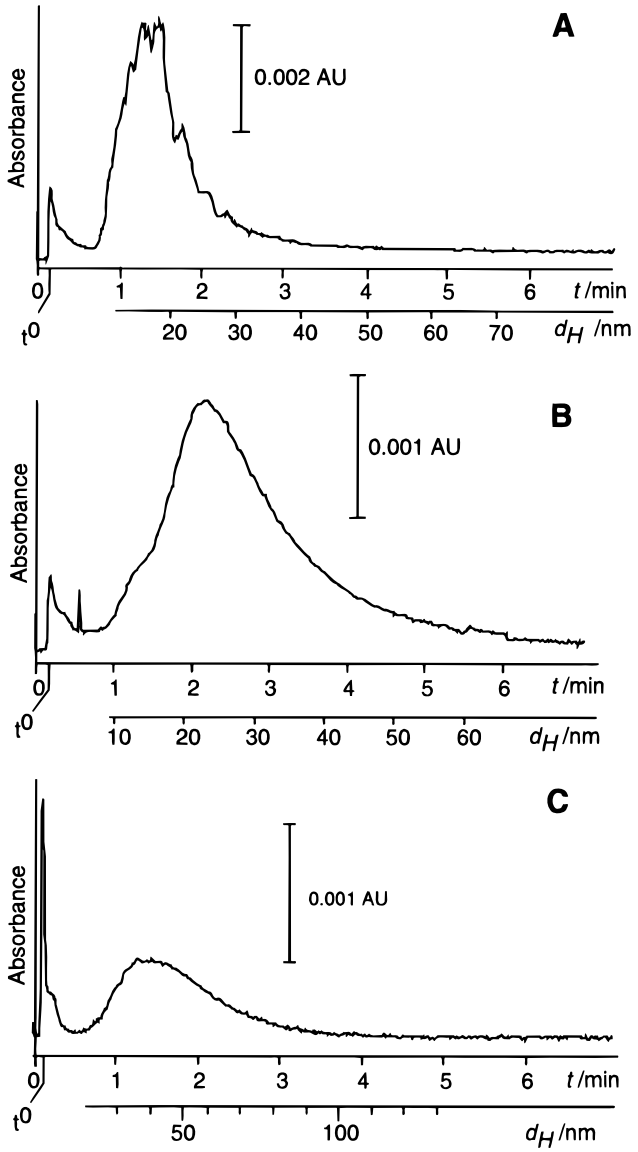

Figure 11. Fractograms of MMA 550 obtained in carriers of 1 mM sodium phosphate buffer of pH 3−9: (A) pH 9.0, V_{in} = 4.0 mL/min, V_{out} = 0.85 mL/min, V_c/V_{out} = 3.2, t^0 = 0.16 min; (B) pH 5.0, V_{in} = 4.0 mL/min, V_{out} = 0.8 mL/min, V_c/V_{out} = 4.0, t^0 = 0.16 min; (C) pH 3.0, V_{in} = 4.0 mL/min, V_{out} = 2.2 mL/min, V_c/V_{out} = 0.8, t^0 = 0.11 min. Sample: MMA 550 diluted in the different carriers to 0.7 mg/mL. The relaxation/focusing time was 1 min.

different shapes of the fractograms if the new medium causes slow changes in those equilibria which influence the polymer size. However, as mentioned above, experiments where the polymer was diluted in alternately water or pH-modified carriers did not result in any differences in the obtained hydrodynamic sizes.

Second, the polymer assumes two concentration profiles inside the channel: one Gaussian profile in the axial direction and one exponential in the transversal direction.[29] Therefore the sample has a maximal concentration at the membrane surface at the center of the Gaussian profile.[27] This maximum concentration will in most practical cases, *i.e.* when complete focusing has been achieved, be in excess of the concentration in the original sample. Thus the concentration conditions prevailing during sample relaxation/focusing and the subsequent elution are different from those in the original sample solution. Concentration effects can of course also be detected by changes in sample concentrations. This caused only a slight change in the position

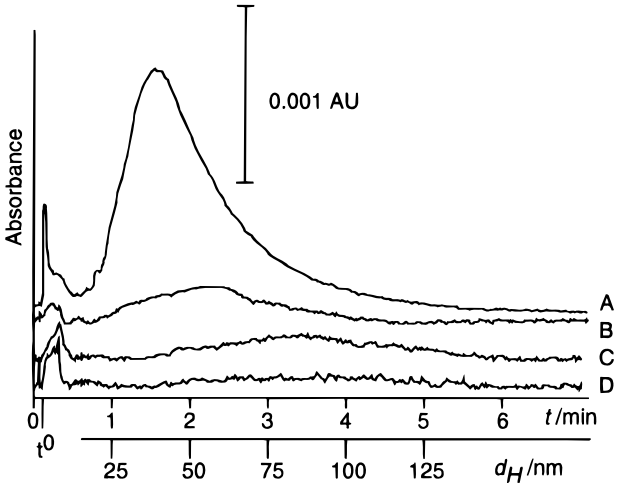

Figure 12. Fractograms of MMA 550 obtained using different relaxation/focusing times in a carrier of 1 mM sodium phosphate buffer, pH 3. Relaxation/focusing times: (A) 1 min, (B) 2 min, (C) 3 min, and (D) 4 min. V_{in} = 4.0 mL/min, V_{out} = 1.1 mL/min, V_c/V_{out} = 2.6, and t^0 = 0.11 min. Sample: MMA 550 diluted in 1 mM sodium phosphate buffer, pH 3, to 0.7 mg/mL.

of the peak occurring in the 3−5 nm range. When the concentration was 1.8 mg/mL instead of 0.7 mg/mL, the observed size was about 1 nm smaller, and this was found for the three pH values from 4.6 and up. Thus, increasing sample concentrations did not result in larger aggregate sizes.

Third, during sample relaxation/focusing, the polymer is held at a stationary position along the membrane while at the same time the exponential concentration layer is being built up (Figure 5). Thus the molecular layer close to the membrane surface has the opportunity to interact with the membrane. Because of the very limited surface area available, it is believed that such effects have little influence on sample migration.[25]

The longer time spent in the focused sample zone during the continuous flushing by the acidic medium seems to favor aggregation, as evidenced by the increased hydrodynamic diameters. The forced conditions prevailing during relaxation/focusing may represent a method to study the tendencies for a polymer to undergo higher order aggregation under certain conditions. It is not clear to us whether the results obtained in acidic medium represent a system at equilibrium or under a continuous change.

As a comparison to the results obtained in dilute HCl and NaOH, pH changes were studied also in media buffered with 1 mM sodium phosphates. These buffers had a low ionic strength (0.002−0.003), yet higher than that in HCl and NaOH of the same pH. Two acidic pH values (5.0 and 3.0) and one alkaline (9.0) were studied. At the high pH, *i.e.* pH 9.0, the polymer backbone would be charged and therefore it would show resistance to backbone interactions. A decrease in pH would decrease the net charge of the backbone, with increased interactions and aggregation as a result. The fractograms obtained using different pH values are shown in Figure 11. The use of pH 9.0 provided a peak with a maximum corresponding to a hydrodynamic diameter of 16 nm. Using lower pH values, the diameter became larger, 23 nm for pH 5.0 and 40 nm for pH 3.0. These sizes are significantly larger than those reported above in dilute HCl and NaOH. Evidently, the change to sodium phosphates caused an increased association tendency at both alkaline and acidic pH values. This may depend on the higher ionic strength.

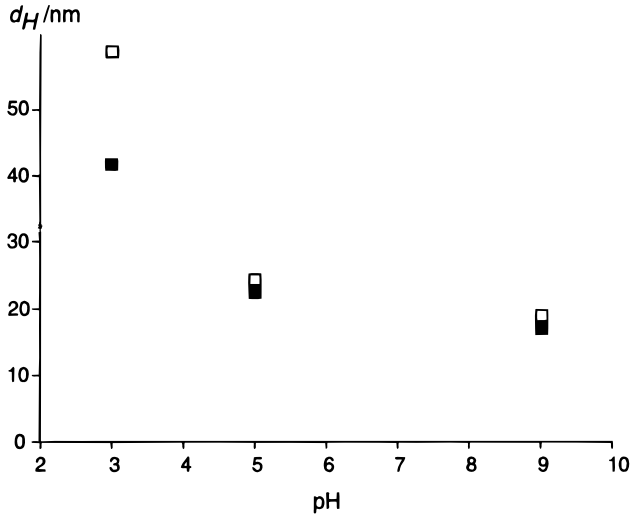

Figure 13. Hydrodynamic diameter as measured at the peak maximum using carrier liquids containing sodium phosphate buffers of pH 3, 5, and 9. Relaxation/focusing times: 1 min (■) and 3 min (□). Sample: MMA 550 diluted in the three different carriers to 0.7 mg/mL.

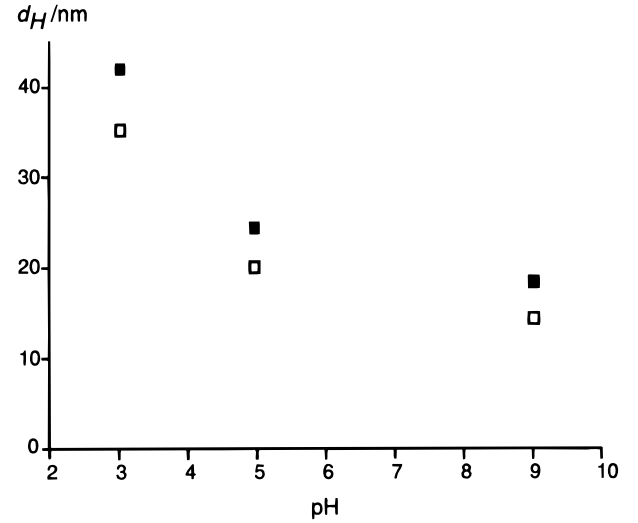

Figure 14. Influence of the sample concentration on the hydrodynamic diameter using carrier liquids containing sodium phosphate buffers of pH 3, 5, and 9. The lower concentration gives somewhat larger diameters. Sample: MMA 550 diluted in the three different carriers to 0.7 mg/mL (■) and 1.8 mg/mL (□). The relaxation/focusing time was 1 min.

As in the experiments with HCl carriers, an increase of the relaxation/focusing time using sodium phosphate buffers caused increases in the observed sizes and, again, the effect is significant at more acidic pH. At pH 9.0 and 5.0, an increase in relaxation/focusing time from 1 to 3 min gave only a very small increase in size (less than 5%), but with pH 3 the size increase is nearly 40% (Figures 12 and 13). According to Figure 12, the peak area decreases dramatically with longer relaxation/focusing times at pH 3. It seems reasonable that with such a low pH the solubility of the polymer was reduced, resulting in formation of very large aggregates which were not eluted from the channel (Figure 12D). The polymer may even have precipitated.

The effects of a change of the sample concentrations at various pH values can be seen in Figure 14. The pattern is similar to the one obtained with the HCl- and NaOH-adjusted carriers above. A lower concentration gave somewhat higher diameter values, and this difference seems to be independent of pH. It has been found that the amount of larger aggregates of a polystyrene−poly(ethylene oxide) block copolymer decreased at higher polymer concentrations.[39] This effect was thought to be related to the complex behavior of the hydrophilic poly(ethylene oxide) in aqueous solution. It is not clear to us if MMA 550 acts in a similar way. Extended studies are needed for further interpretations of the concentration effects.

Acknowledgment. This study was supported by grants from the Swedish Research Council for Engineering Sciences. The development of the FFF system was made possible by grants from the Astra Hässle AB and the Crafoord Foundation. Mr. Stefan Magnusson is gratefully acknowledged for experimental assistance.

References and Notes

(1) Wesslén, B.; Wesslén, K. B. *J. Polym. Sci.* **1992**, *30*, 355.
(2) Wesslén, K. B. Licentiate thesis, University of Lund, 1991.
(3) Tuzar, Z.; Kratochvil, P. *Adv. Colloid Interface Sci.* **1976**, *6*, 201.
(4) Lindman, B.; Wennerström, H. *Top. Curr. Chem.* **1980**, *87*, 1.
(5) Piirma, I. *Surf. Sci. Ser.* **1992**, *42*, 49.
(6) Hamad, E.; Qutubuddin, S. *Macromolecules* **1990**, *23*, 4185.
(7) Valint, P. L.; Bock, J. *Macromolecules* **1988**, *21*, 175.
(8) Price, C. *Pure Appl. Chem.* **1983**, *10*, 1563.
(9) Nwankwo, I.; Xia, D.; Smid, J. *J. Polym. Sci.* **1988**, *26*, 581.
(10) Boucher, E. A.; Hines, P. M. *J. Polym. Sci.* **1976**, *14*, 2241.
(11) Florin, E.; Kjellander, R.; Eriksson, J. C. *J. Chem. Soc.* **1984**, *80*, 2889.
(12) Kjellander, R.; Florin, E. *J. Chem. Soc.* **1981**, *77*, 2053.
(13) Weiner, B. B.; Tscarnuter, W. W. In *Uses and Abuses of Photon Correlation Spectroscopy in Particle Sizing*; Prowder, T., Ed.; ACS Symposium Series 332; American Chemical Society: Washington, DC, 1987; Chapter 3.
(14) Bott, S. E. In *Submicrometer Particle Sizing by Photon Correlation Spectroscopy*: *Use of Multiple Angle Detection*; Prowder, T., Ed.; ACS Symposium Series 332; American Chemical Society: Washington, DC, 1987; Chapter 5.
(15) Koehler, M. E.; Prowder, T. In *Comparative Particle Size Analysis*; Prowder, T., Ed.; ACS Symposium Series 332; American Chemical Society: Washington, DC, 1987; Chapter 16.
(16) Giddings, J. C. *Sep. Sci.* **1966**, *1*, 123.
(17) Giddings, J. C. *Science* **1993**, *260*, 1456.
(18) Chen, X.; Wahlund, K.-G.; Giddings, J. C. *Anal. Chem.* **1988**, *60*, 362.
(19) Litzén, A.; Wahlund, K.-G. *J. Chromatogr.* **1991**, *548*, 393.
(20) Wahlund, K.-G.; Litzén, A. *J. Chromatogr.* **1989**, *461*, 73.
(21) Litzén, A.; Walther, J. K.; Krischollek, H.; Wahlund, K.-G. *Anal. Biochem.* **1993**, *212*, 469.
(22) Wahlund, K.-G.; Winegarner, H. S.; Caldwell, K. D.; Giddings, J. C. *Anal. Chem.* **1986**, *58*, 573.
(23) Kirkland, J. J.; Dilks, C. H.; Rementer, S. W. *Anal. Chem.* **1992**, *64*, 1295.
(24) Giddings, J. C.; Benincasa, M. A.; Liu, M.-K.; Li, P. *J. Liq. Chromatogr.* **1992**, *15*, 1729.
(25) Giddings, J. C.; Benincasa, M. A. *Anal. Chem.* **1992**, *64*, 790.
(26) Kirkland, J. J.; Dilks, C. H. *Anal. Chem.* **1992**, *64*, 2836.
(27) Caldwell, K. D.; Brimhall, S. L.; Gao, Y.; Giddings, J. C. *J. Appl. Polym. Sci.* **1988**, *36*, 703.
(28) Xu, R.; Hu, Y.; Winnik, M. A.; Riess, G.; Croucher, M. D. *J. Chromatogr.* **1991**, *547*, 434.
(29) Wahlund, K.-G.; Giddings, J. C. *Anal. Chem.* **1987**, *59*, 1332.
(30) Litzén, A.; Wahlund, K.-G. *Anal. Chem.* **1991**, *63*, 1001.
(31) Litzén, A. *Anal. Chem.* **1993**, *65*, 461.
(32) Ratanathanawongs, S. K.; Giddings, J. C. *Anal. Chem.* **1992**, *64*, 6.
(33) Liu, M.-K.; Giddings, J. C. *Macromolecules* **1993**, *26*, 3576.
(34) Giddings, J. C.; Lin, G.-C.; Myers, M. N. *J. Colloid Interface Sci.* **1978**, *65*, 67.
(35) Dérand, H.; Wesslén, B. *J. Polym. Sci., Part A* **1995**, *33*, 571.
(36) Litzén, A. Doctoral Dissertation, University of Uppsala, 1992.
(37) Bekturov, E. A.; Bakunova, Z. K. *Synthetic Water-soluble Polymers in Solution*; Hüthig und Wepf Verlag: Heidelberg, 1986; Chapter 4.
(38) Berlinova, I. V.; Vladimirov, N. G.; Panayotov, I. M. *Makromol. Chem. Rapid Commun.* **1989**, 162.
(39) Xu, R.; Winnik, M. A. *Macromolecules* **1991**, *24*, 87.

MA950837S